JOURNAL OF SPACECRAFT AND ROCKETS
Vol. 45, No. 2, March–April 2008

Free-Molecule-Microresistojet Performance Using Water Propellant for Nanosatellite Applications

R. H. Lee,* A. M. Bauer,† M. D. Killingsworth,‡ T. C. Lilly,§ and J. A. Duncan†
University of Southern California, Los Angeles, Los Angeles California 90089-1191
and
A. D Ketsdever¶
U.S. Air Force Research Laboratory, Edwards Air Force Base, California 93524

DOI: 10.2514/1.32341

Advances in microtechnology manufacturing and capability have led to an increased interest in micro- and nanosatellites. A propulsion system was designed to meet the on-orbit attitude control requirements for nanospacecraft. The free-molecule microresistojet, a low-cost, low-power, high propellant-storage density, and green propulsion system, was analyzed in this study to determine its ability to provide a slew maneuver for a typical 10-kg nanosatellite. Additionally, a free-molecule-microresistojet technology demonstrator was fabricated using traditional and microelectromechanical systems techniques. The technology demonstrator was analyzed and tested in this study to determine its performance characteristics when operating with water propellant. Experimental data show that the free-molecule microresistojet, with a heated wall temperature of 580 K, can attain a specific impulse of 79.2 s with a thrust level of 129 μN. For a given mass flow, higher thrust levels can be achieved by increasing the temperature of the free-molecule-microresistojet heater chip. The experimental results agree favorably with predicted values from kinetic theory. Applying the measured performance of the technology demonstrator to an optimized setup, the free-molecule-microresistojet system could provide a 45-deg slew of a typical nanosatellite in 60 s, which is acceptable for many nanosatellite applications.

Nomenclature

A_s = area of the expansion slots, m^2
C = mass flow rate constant, m · s
D_{pore} = diameter of the pore, m
F_{dyn} = fluid dynamic force, N
F_{st} = surface tension force, N
g_o = gravitational constant (9.81 m/s^2)
h_e = height of the empty cavity, m
h_p = height of the propellant, m
I_{sp} = specific impulse, s
I_{tot} = total impulse, s
k = Boltzmann's constant (1.38E-23 J/K)
m = molecular mass, kg
M = total mass of the satellite, kg
m_w = mass of the sloshing wave, kg
m_{prop} = mass of the propellant, kg
P_o = stagnation pressure, bar
P_{vap} = vapor pressure, bar
r_t = radius of the propellant tank, m
T_o = stagnation temperature, K
T_w = expansion-slot wall temperature, K
V_e = volume of the empty cavity, m^3
α = transmission probability
γ = surface tension of water, dyne/m
θ = contact angle, deg

Presented as Paper 5185 at the AIAA 43rd Joint Propulsion Conference, Cincinnati, OH; received 24 May 2007; revision received 17 September 2007; accepted for publication 22 September 2007.

*Graduate Research Assistant, Astronautics and Space Technology Division. Student Member AIAA.
†Undergraduate Research Assistant, Department of Aerospace and Mechanical Engineering. Student Member AIAA.
‡Undergraduate Research Assistant, Astronautics and Space Technology Division. Student Member AIAA.
§Graduate Research Assistant, Department of Aerospace and Mechanical Engineering. Student Member AIAA.
¶Group Leader, Aerophysics Branch, Propulsion Directorate. Senior Member AIAA.

I. Introduction

NANOSATELLITE missions are currently being conceived as a result of the development of micro- and nanotechnologies. The general agreement in the spacecraft community is that a nanosatellite represents a total system mass between 1 and 10 kg [1]. Nanosatellites impose significant limitations on the mass, power, and volume available for all subsystems, including propulsion [2]. The presence of such a propulsion system will allow orbit maintenance, pointing-angle adjustments, or formation repositioning. Figure 1 shows the thrust versus the maneuver time required for various pointing-angle adjustments. These slew maneuvers assume a 10-kg cylindrical nanosatellite of consistent density. The satellite was defined as consisting of 30% aluminum covering the structures, whereas the remainder of the satellite was silicon, based on the requirement for microelectromechanical system (MEMS) fabrication. The nanosatellite was assumed to be 14.50 cm in diameter and 24.92 cm in height, giving a moment of inertia about the spin axis of 0.0263 kg · m^2. As seen in Fig. 1, thrusters can provide a 45-deg slew in 60 s at a thrust level of 0.3 mN. According to Janson et al. [3], a slew on the order of tens of seconds would be considered to be a relatively quick maneuver. Although propulsion systems can prove to be enabling for nanosatellite missions, many current systems are too massive and draw too much power for consideration on nanosatellites [2].

The free-molecule microresistojet (FMMR) was designed to meet the strict requirements of nanosatellites [4]. The FMMR exhibits many system features that are beneficial to nanosatellite operations, including low-pressure operation, low power consumption, low mass, and low propellant-storage volume. The FMMR's ability to operate on lower pressures permits the use of a propellant stored as either a liquid or solid at nominal storage temperatures. The storage density of the propellant is important to minimize the volume required for the propellant tanks. In this study, the performance of the FMMR with a liquid water propellant is of interest. Several factors were identified that make the use of water propellant beneficial to the

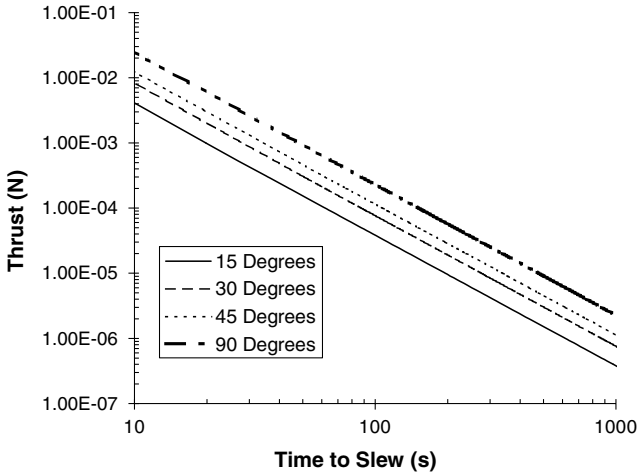

Fig. 1 Thrust versus maneuver time for a typical nanosatellite slew; the moment of inertia is 0.0236 kg · m^2 and the radius is 0.0725 m.

FMMR system. First, water is stored as a liquid onboard the nanosatellite, with a relatively high storage density compared with gaseous propellants. Second, water has a relatively low molecular mass, which enhances the specific impulse for electrothermal thrusters. Third, water has a relatively high vapor pressure at typical nanosatellite on-orbit temperatures. The vapor pressure is sufficient to provide FMMR operating pressures without the need to prevaporize the liquid propellant. Finally, water's surface tension allows for phase separation with a hydrophobic microporous membrane, to insure that only gaseous propellant makes it to the FMMR plenum.

The FMMR consists of three main parts: the heater chip, the flow control, and the propellant storage. These parts are shown in Fig. 2 for an optimized nanosatellite propulsion system. The propellant gas arrives in the plenum after passing through a set of phase-separating filters and an actuating valve. The FMMR generates thrust by expelling the propellant gas in the plenum through a series of the expansion slots in the MEMS-fabricated heater chip.

Although the FMMR system illustrated in Fig. 2 is optimized for a nanosatellite, a technology demonstrator (TD) was fabricated using traditional and MEMS techniques. The TD is shown in Fig. 3. This system was designed to perform a spin maneuver on a university microsatellite [3]. Because the thrust requirement for the microsatellite was significantly larger than for a typical nanosatellite, the TD design was driven by factors not necessarily consistent with the FMMR concept. However, the FMMR was scalable and offered a reasonable propulsion system for the 25-kg-class satellite. The TD also offered a reduced cost of fabrication, easier performance testing of the system, and met all of the flight safety requirements for a payload flying on modern launch vehicles.

The FMMR heater chips for the optimized and TD systems are shown in Fig. 4. The TD heater chip is significantly larger, for the purpose of producing a larger thrust level. This shows the flexibility of the FMMR system for satellite design. By adding expansion slots and thus increasing the propellant mass flow, the FMMR system can be tuned to the thrust level required by a particular mission. The expansion-slot design also leads to a reduction in possible single-point failures over the expansion of the propellant through a traditional single-nozzle configuration. A high-pressure nozzle expansion, producing thrust comparable with FMMR, would be limited by a relatively small throat diameter. Plugging of the throat by a contaminant could lead to a failure; however, the plugging of a portion of a slot would still leave the remaining slot area available for thrust generation. A potential drawback of the expansion-slot design is the loss of propulsive efficiency over a contoured-nozzle design. However, a previous study showed that for low-Reynolds-number operation (consistent with the FMMR design), a nozzle does not offer a distinct enhancement in performance over a simple orifice or slot [5].

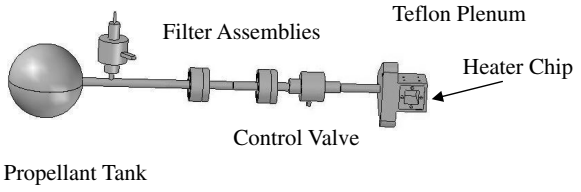

Fig. 2 Optimized nanosatellite FMMR propulsion system.

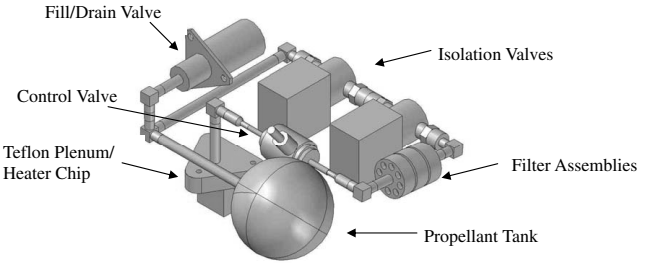

Fig. 3 Technology-demonstration FMMR (flight version).

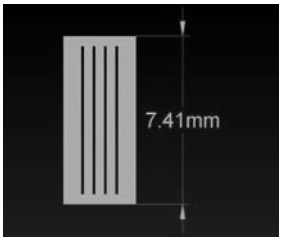

a)

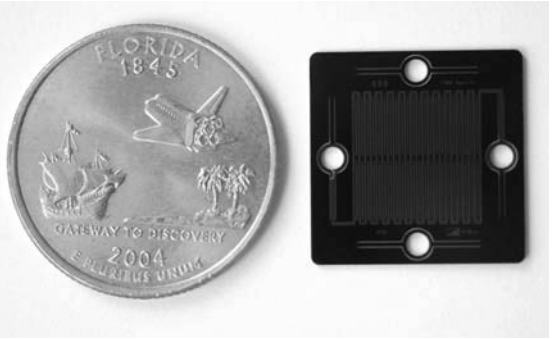

b)

Fig. 4 Top view of the FMMR heater chip: a) optimized for a typical nanosatellite and b) technology-demonstration version.

II. System Configuration

Figure 3 shows the flight version of the technology-demonstration FMMR that was described in detail in [4]. The TD system consists of a stainless steel propellant tank, a service (fill/drain) valve, two one-time latching valves, a phase-separation housing, an actuating valve, and a Teflon plenum onto which the heater chip is mounted. The propellant tank is 63.11 mm in diameter, which is capable of holding 130 g of water propellant. The propellant tank has a burst pressure of 5.17 MPa, making it far heavier than a low-pressure FMMR system would actually require. The two latching valves are required for mechanical inhibits by the launch vehicle. The latching valves on the TD were selected for their low cost and relatively low power. For the optimized nanosatellite version, these valves could be replaced by one-time MEMS isolation valves described by Mueller et al. [6], which would significantly reduce the mass and volume used to inhibit the flow during the launch phase.

The TD phase-separation housing consists of two membranes, to insure only water vapor reaches the plenum and heater chip. Water

propellant is restricted from flowing past the membranes by surface tension forces. Teflon microporous membranes are used due to their hydrophobic nature, with the pore size determined by the worst-case propellant tank operating pressure. Because of the high mass flow required for the TD, the phase-separation housing shown in Fig. 3 is relatively large. The distance between the actuating valve and the plenum in the TD led to the use of two microporous membranes. The second membrane reduces the possibility of water propellant condensing in the propellant feed system between the actuating valve and the plenum. In the optimized nanosatellite design, the housing size could be minimized with the use of a single membrane, due to the short distance expected between the housing and the plenum with a typical microvalve. The phase separator also serves as a filter system to remove particulates.

The TD actuating valve was selected because of its flight heritage and relatively low power consumption. As the only moving part during the flight demonstration phase, it was critical to have a component with flight heritage to increase the reliability of the overall propulsion system. For the optimized nanosatellite design, a microscale valve would be used, such as the piezoelectric valve described by Yang et al. [7] or the thermopneumatic valve described by Henning et al. [8]. Although the development of microvalves has been ongoing, suitable valves for micropropulsion systems remain elusive. For power-limited nanosatellites, low-power microvalves are required. In the particular case of low-pressure FMMR operation, microvalves with relatively large orifice diameters are required, complicating design. Although a notional optimized FMMR design can be conceived, a suitable microvalve has not been identified.

Teflon is the material of choice for the FMMR plenum, due to its inherently low thermal conductivity. In optimized designs, Pyrex plenums may be ideal, because the silicon heater chips can be directly bonded (anodically) to the plenum. For smaller heater chips resulting in lower-power operation than the TD, the heat transfer from the chip to the plenum could be reasonably reduced, making Pyrex more attractive. Initial results indicate that anodic bonding between a silicon heater chip and a Pyrex plenum for chip temperatures up to 700 K did not result in failure due to stresses formed by differential thermal expansion. Figure 4 shows the optimized FMMR heater chip. Note that the attachment holes for mechanical mating to the plenum on the TD version are removed as a result of the anodic bonding.

The operating characteristics of the TD and the optimized nanosatellite FMMR are given in Table 1. The power required for the heater chip in the optimized design was derived from area scaling of the measured TD values. Therefore, the estimates for the power to the optimized design are considered to be reasonably conservative. The system-preparation power shown in Table 1 indicates the necessity to actuate the one-time inhibit valves before general operation of the thruster can commence. For the TD, the two inhibit valves are actuated and latched in series, resulting in two separate system-preparation periods. These periods can be temporally spaced to meet driving satellite power requirements. The transient power required for the FMMR represents the initial power draw of the actuating valve and heater chip, which eventually reach ($\sim$20 ms for the valve and $\sim$1 min for the heater chip) a steady-state power draw. Component masses for the TD and an optimized design are given in Table 2.

Table 1 FMMR operating characteristics

	System-preparation power, W	Transient power, W	Steady-state power, W
Technology demonstrator			
Inhibit valves	9	n/a	n/a
Actuating valve	n/a	4.36	1
Heater chip	n/a	5	3.2
Optimized nanosatellite design			
Inhibit valves	1	n/a	n/a
Actuating valve	n/a	<1	<1
Heater chip	n/a	1	0.22

Table 2 FMMR system mass

	TD mass, g	Optimized mass, g
Actuating control valve	130	<10
Fill/drain valve	150	<10
Inhibit valves (x2)	353	<20
Plenum, heater chip, mounting	87	35
Phase-separation system	110	35
Feed lines	92	5
Propellant tank	50	10
Propellant	90	90
Total	1062	175

III. Theory

A. FMMR Performance

The performance of the FMMR has been theoretically analyzed elsewhere as a free-molecule flow of the propellant through the expansion slots [4]. This previous study has shown that the measured specific impulse for the FMMR is generally 10–15% higher than the analytical predictions for gaseous propellants. The major reason for the difference is that the FMMR operating range is in the transitional flow regime and not in the free-molecule flow regime. Higher-pressure operation would lead to more efficient thruster operation, but this trend is counteracted by the propellant tank mass and the leak rate of available microvalves [9].

B. Propellant Slosh

The effect of slosh in a liquid propellant can be detrimental to a stabilized satellite. If the mass of the sloshing waves is too large, the satellite could begin to nutate. The mass of the sloshing waves is a function of the height of the propellant and the radius of the propellant tank. The volume of the empty portion of a spherical propellant tank is given by

$$V_e = \tfrac{1}{3}\pi h_e^2(3r_t + h_e) \tag{1}$$

where the resulting height of the propellant is

$$h_p = 2r_t - h_e \tag{2}$$

A correlation between h_p/r_t and m_w/M is found in [10]. For the parameters of the TD, the resulting mass of the sloshing waves before the burn maneuver and after half of the propellant has been used is 22.5 g for both cases. Even in the worst-case scenario in which the entire propellant is sloshing ($m_w = m_{\text{prop}}$), the mass of the sloshing wave is well below 1% of the total satellite mass for the TD mission. According to Bauer [11], the effect of the propellant slosh on satellite attitude should be minimal.

C. Propellant Phase Separation

Microporous membranes are used in the FMMR system to remove particulate contaminants and to achieve propellant phase separation. Water propellant is stored as a liquid in the propellant tank. The thruster operates by expanding water vapor through the expansion slots. Because nanosatellites are extremely power-limited, the power required to actively vaporize the liquid water propellant would be prohibitive. For the FMMR, phase separation is accomplished through surface tension forces between the liquid water propellant and a hydrophobic (nonwetting) porous material. The surface tension force is given by

$$F_{\text{st}} = \pi D_{\text{pore}}\gamma(T)\cos\theta \tag{3}$$

For a hydrophobic Teflon material, the contact angle is 110 deg [12].

The competing fluid dynamic force trying to force liquid water through the Teflon membrane is given by

$$F_{\text{dyn}} = P_{\text{vap}}(T)\left(\frac{\pi D_{\text{pore}}^2}{4}\right) \tag{4}$$

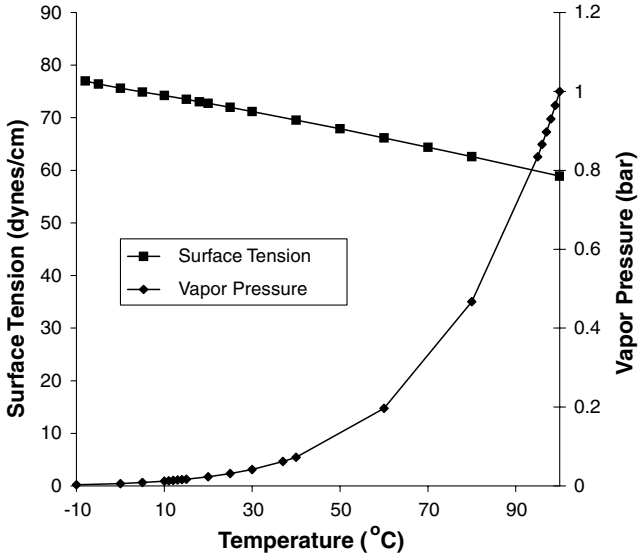

Fig. 5 Surface tension and vapor pressure of water as a function of temperature.

The pore size in the phase-separating Teflon membrane was determined from the worst-case pressure in the propellant tank. In this case, the design requirement is for the microporous membrane to restrict the liquid water from passing through the membrane, or $F_{\text{st}} \geq F_{\text{dyn}}$. Therefore,

$$D_{\text{pore}} \leq \left| \frac{4\gamma(T)\cos\theta}{P_{\text{vap}}(T)} \right| \tag{5}$$

The surface tension and vapor pressure of water as a function of temperature is shown in Fig. 5 [13]. From the worst-case scenario from the TD mission ($T = 30°\text{C}$), D_{pore} from Eq. (5) should be less than or equal to 23.3 μm. For the design of the actual TD, the pore size was selected to be 1 μm, due to its ready availability.

Evaporative cooling could lead to the propellant menisci freezing in the micropores. The current TD does not have active heating of the propellant tank, feed lines, or phase-separation system. Instead, integration control has placed the phase-separating membranes in an area in which waste heat exists from nearby electronic components. Although the availability of waste heat is not a strict requirement for the TD or any future versions of the FMMR system, advantage is taken of its availability for critical components such as the phase-separation system.

IV. Experimental Setup

The propulsive characteristics of the FMMR were measured using the nano-Newton thrust stand (nNTS) with an electrostatic comb calibration system, described in detail elsewhere [14,15]. The operation of the nNTS was performed in chamber-IV of the Collaborative High-Altitude Flow Facility (CHAFF-IV) at the University of Southern California. CHAFF-IV was capable of maintaining background pressures below 10^{-5} torr throughout the range of experiments performed in this study. Maintaining low background pressure was critical in obtaining accurate thrust measurements [16].

For the thrust measurements involving water, propellant was fed from a chilled vacuum-insulated container that brought the propellant to a stable temperature of approximately 0°C, corresponding to a stable vapor pressure of approximately 4.6 torr. Standard Venturi mass flow meters did not produce accurate results for the relatively low water vapor flow rates investigated here. The mass flow of the propellant was instead determined from recorded stagnation pressures in the plenum over the flow period and extrapolating a mass flow. From the theoretical model [4], we can take the mass flow to be the time rate of change of the mass of the propellant, which yields

$$\frac{\mathrm{d}m_p}{\mathrm{d}t} = \alpha P_0 \sqrt{\frac{M}{2\pi k T_0}} A_s \tag{6}$$

For a given temperature, the right-hand side of the equation is directly proportional to the pressure. The integration of both sides of Eq. (6) over the time of the trace gives a relation for the total mass loss and the plenum pressure:

$$\Delta m_p|_o^t = C \int_0^t P_0 \,\mathrm{d}t \tag{7}$$

where C is the constant defined as

$$C = \alpha \sqrt{\frac{M}{2\pi k T_0}} A_s \tag{8}$$

Because the transmission probability a is not known a priori, the value of C must be found experimentally. The constant C can be experimentally determined though Eq. (7) by measuring the total mass loss of the propellant over a specified time and dividing by the integral of the pressure in the plenum over that time. The experimental setup for determining C consisted of connecting a sealable 2-cm-diam bulb of liquid water to the FMMR plenum. A valve between the bulb and the plenum was opened for a time period of several hours. As the water vapor flowed to the plenum, it caused both an aggregate loss of fluid in the bulb and a measurable pressure in the plenum. The mass change in the bulb was measured with a precision of ± 0.1 mg. The pressure in the plenum was also recorded to measure its variation as a function of time. The time-integral of the plenum pressure was approximated using a standard trapezoidal Riemann sum over all of the data, and this integral was compared against the associated mass loss for each trace to determine the constant C. Once C is determined, the specific impulse is found through

$$I_{\text{sp}} = \frac{I_{\text{tot}}}{g_0 C \int_0^t P_0 \,\mathrm{d}t} \tag{9}$$

The experimental setup for thrust testing was such that P_o could not be directly recorded simultaneously with thrust, due to the movement of the nNTS. However, rigorous testing proved that for a given T_o, a proportional relationship exists between P_o and the pressure recorded upstream from the plenum, P_1. This relationship was experimentally established using a static plenum at a nominal chip temperature $T_o = 300$ K. It was experimentally determined that at a constant position upstream of the plenum, P_1 was only dependent on the mass flow through the system and not on T_o.

The burst-pressure characteristics of the Teflon phase-separating membranes were tested by placing the filter in a housing with liquid water on one side and atmosphere on the other. The liquid water column was pressurized as each membrane was tested to failure, a condition that was defined and observed when a single drop of liquid water was forced through the membrane. If liquid water were to bypass the membrane, it would likely freeze in the feed system or in the heater-chip expansion slots, causing unpredictable and uncontrollable thrust as it sublimated.

V. Results and Discussion

As mentioned earlier, the current version of the FMMR was designed for technology demonstration on a university microsatellite. As such, it was critical to fully characterize its performance using water propellant, which will be used on the mission. These results were also applied to the optimized nanosatellite FMMR design to lend some basis for the estimation of thermal and propulsive characteristics. To establish that the FMMR design meets both the transient and steady-state power requirements for the proposed technology-demonstration mission, experiments were performed to measure thermal characteristics of the heater chip and plenum assembly. The heater-chip temperature is shown in Fig. 6 as a function of the input power. The data were taken for a propellant flow

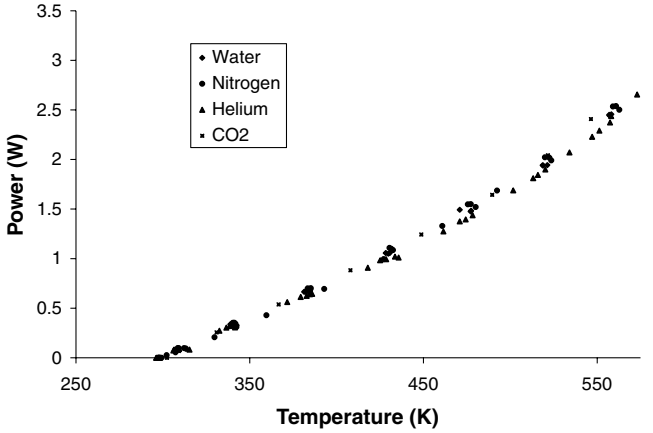

Fig. 6 Input power versus heater-chip temperature.

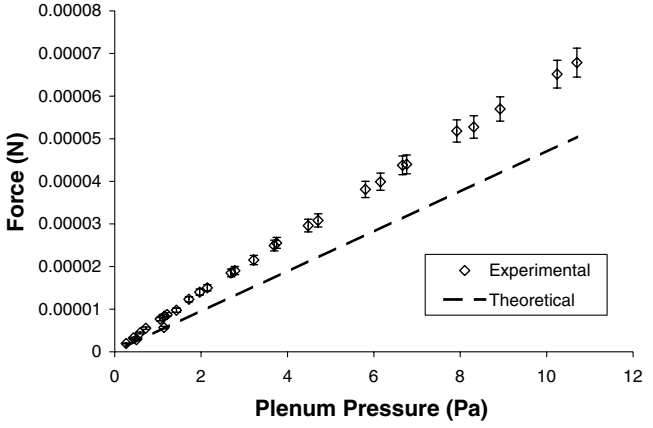

Fig. 7 Experimental and theoretical thrust as a function of H_2O pressure.

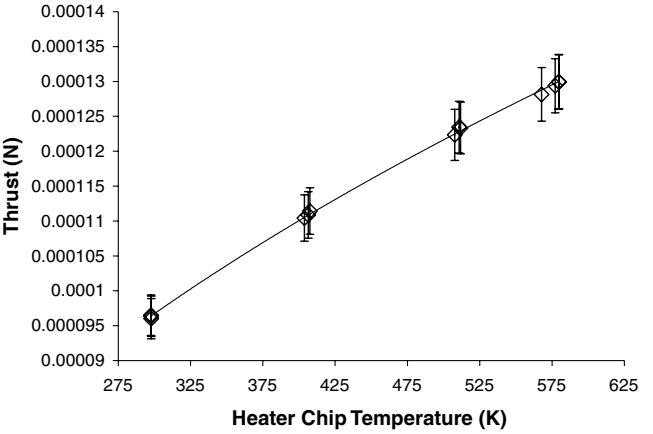

Fig. 8 Thrust versus heater-chip temperature for H_2O propellant.

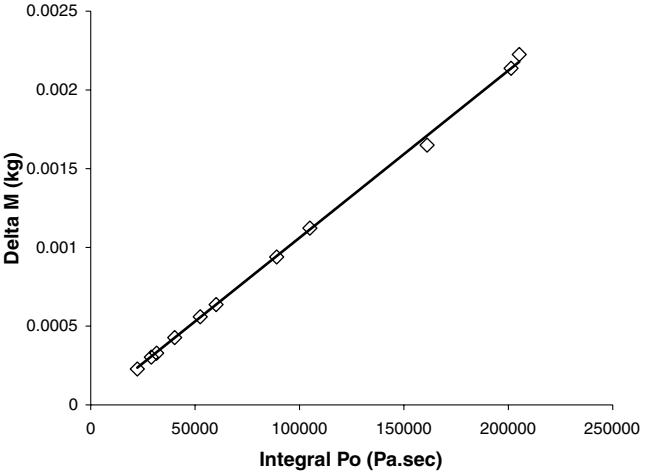

Fig. 9 Mass used as a function of the integral of plenum pressure with time.

rate of 10 sccm (the mass flow expected in orbit) using various propellants. As shown in Fig. 6, the power requirement for the FMMR heater chip is fairly independent of the propellant being used.

Figure 7 shows the experimental and theoretical thrust versus the plenum pressure. As Fig. 7 indicates, the experimental thrust trends toward the theory line at low pressure. As stated in [4], the theory developed assumes free-molecule flow with $Kn \gg 1$. For the pressure and temperature range in Fig. 7, the water Knudsen number ranges from 1 to 0.3, based on the stagnation number density and expansion-slot width. This is classified as the transitional flow regime [17] for which there is no analytical solution. The low Knudsen numbers imply that the FMMR flows for these conditions are not free-molecular and that there are a significant number of collisions between propellant molecules. As the FMMR plenum pressure increases, a continuum flow regime is approached ($Kn \ll 1$) and the transport of momentum through the expansion slots is expected to become more efficient [5]. The optimum performance of the FMMR is a trade between higher efficiency at higher operating pressure and the systems complications that high pressure entails. High pressures in the propulsion system could lead to the complications of massive propellant tanks, high power vaporization of the propellant, or MEMS valve leakage [9].

Figure 8 shows the thrust of the FMMR using water as a function of the heater-chip temperature T_w for a constant mass flow rate of 1.72×10^{-7} kg/s (14-sccm flow rate). From the theoretical model, the relationship between thrust and the heater-chip temperature is expected to vary as $\sqrt{T_w}$, which is consistent for the water propellant data. Figure 9 shows the total water propellant mass used as a function of the integral of the plenum pressure with time. The slope of the line in Fig. 9 gives the constant $C = 1.062 \times 10^{-8}$ [Eq. (7)]. Figure 10 shows the specific impulse as a function of heater-chip temperature T_w for various propellants. As with higher-pressure propulsion systems, the free-molecule theoretical model also predicts the specific impulse to vary as $\sqrt{T_w/m}$.

As shown in Fig. 10, the specific impulse for water lies between the data for helium and nitrogen, as expected for the entire range of heater-chip temperatures. At the operating heater-chip temperature expected for the TD ($T_w = 580$ K), the specific impulse was measured to be 79.2 s. The results in Fig. 8 indicate that some level of thrust control can be obtained by varying the heater-chip temperature. However, the heater-chip temperature is obviously tied to the propulsion system power, as shown in Fig. 6, and

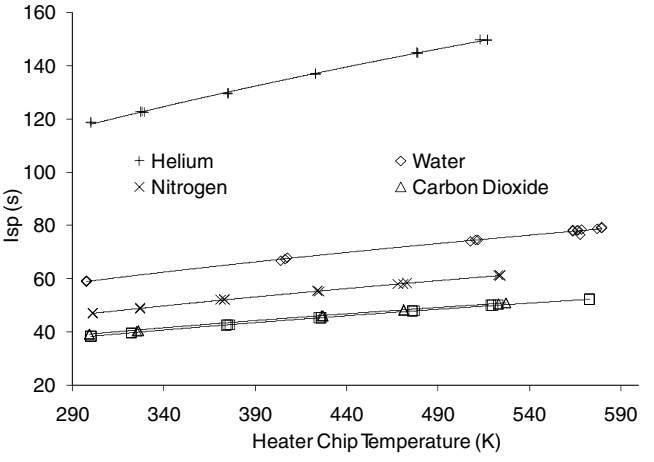

Fig. 10 Specific impulse versus heater-chip temperature.

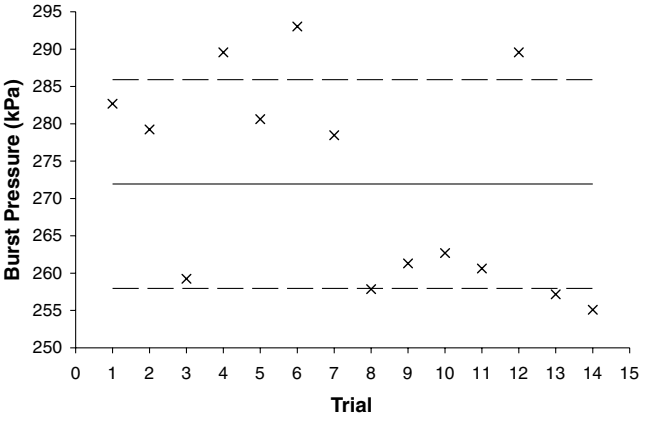

Fig. 11 Burst-pressure test results for phase-separating membranes.

temperature variations can impact the propulsion system power by several watts. In addition, the heater-chip temperature is also tied to the overall specific impulse, as shown in Fig. 10. Reduced-temperature operation to reduce the thrust produced can lead to a lower specific impulse and potentially lower thruster efficiencies.

The results of several burst tests on the phase-separating membranes are shown in Fig. 11. The average pressure that induced a membrane failure was 272 kPa. Considering the internal temperature of a typical nanosatellite, the vapor pressure of a water propellant could reach as high as 13.5 kPa, giving a factor of safety of almost 20. Phase-separating membranes with a larger pore diameter could lead to an increase in the membrane open area, increasing the maximum flow rate through the membrane.

The TD FMMR was designed to meet the requirements of a relatively high-mass nanosatellite. To show utility in the technology demonstration, a relatively large thrust was required to spin up the nanosatellite within a time period acceptable to the overall mission architecture. The large thrust level and required secondary payload safety requirements drove the design and efficiency of the propulsion system. The technology demonstration has several success criteria, including the successful operation of the MEMS-fabricated heater-chip, demonstration of the phase-separating membranes, and demonstration of a thrust level capable of spinning up the nanosatellite. The success criteria drove the use of commercial-off-the-shelf (COTS) valves due to reliability issues and a lack of flight heritage associated with microvalves. The use of COTS valves dramatically increased the propulsion system's mass and power requirements. Future designs capable of propulsive efficiencies on the order of 30% have been envisioned and are shown as the optimum design in Table 1 and Figs. 2 and 4. These future designs include MEMS-fabricated valves and system integration consistent with MEMS fabrication techniques.

VI. Conclusions

For propulsion, the limited resources of a typical nanosatellite result in a trade between the desired performance (thrust and specific impulse) and the required power. This trade space was experimentally investigated for the FMMR using a typical nanosatellite design, and the system can provide a 45-deg slew in 60 s, a time considered to be reasonably fast for nanosatellite maneuvers. Additionally, the technology-demonstration FMMR was fully characterized in this study using water as a propellant. The data obtained from the experiments adhere reasonably well to theory. At the current operating temperature and pressure, the TD produces 129 μN with a specific impulse of 79.2 s. The mass of sloshing waves in the propellant is well below the value considered to be detrimental to the stability of a stabilized satellite. For the TD FMMR, a phase-separating membrane was needed to ensure that the water propellant reaches the plenum in the gaseous phase. The burst pressure of the phase-separating membranes is well above the normal operating pressure of the thruster, resulting in a factor of safety of approximately 20.

Acknowledgments

This work was supported by the Propulsion Directorate of the U.S. Air Force Research Laboratory at Edwards Air Force Base. The authors wish to thank Mike Huggins and Ingrid Wysong for their continued support. The authors are also indebted to Stephen Vargo for his efforts in assisting with the design and fabrication of the free-molecule-microresistojet heater chip.

References

[1] Ketsdever, A., "System Considerations and Design Options for Microspacecraft Propulsion Systems," *Micropropulsion for Small Spacecraft*, edited by M. Micci and A. Ketsdever, Progress in Astronautics and Aeronautics, Vol. 187, AIAA, Reston, VA, 2000, pp. 139–163.

[2] Mueller, J., "Thruster Options for Microspacecraft: A Review and Evaluation of State-of-the-Art and Emerging Technologies," *Micropropulsion for Small Spacecraft*, edited by M. Micci and A. Ketsdever, Progress in Astronautics and Aeronautics, Vol. 187, AIAA, Reston, VA, 2000, pp. 45–137.

[3] Janson, S., Helvajian, H., Hansen, W., and Lodmell, J., "Microthrusters for Nanosatellites," *The Second International Conference on Integrated Micro Nanotechnology for Space Applications (MNT99)*, The Aerospace Corp., El Segundo, CA, Apr. 1999.

[4] Ketsdever, A., Lee, R., and Lilly, T., "Performance Testing of a Microfabricated Propulsion System for Nanosatellite Applications," *Journal of Micromechanics and Microengineering*, Vol. 15, No. 12, 2005, pp. 2254–2263. doi:10.1088/0960-1317/15/12/007

[5] Ketsdever, A., Clabough, M., Gimelshein, S., and Alexeenko, A., "Experimental and Numerical Determination of Micropropulsion Device Efficiencies at Low Reynolds Number," *AIAA Journal*, Vol. 43, No. 3, 2005, pp. 633–641.

[6] Mueller, J., Vargo, S., Green, A., Bame, D., Orens, R., and Roe, L., "Development of a Micro-Isolation Valve: Minimum Energy Requirements, Repeatability of Actuation, and Preliminary Studies of Debris Generation," 36th Joint Propulsion Conference, Huntsville, AL, AIAA Paper 2000-3675, 2000.

[7] Yang, E., Rohatgi, N., and Wild, L., "A Piezoelectric Microvalve for Micropropulsion," NanoTech 2002 Conference, Houston, TX, AIAA Paper 2002-5713, Sept. 2002.

[8] Henning, A. K., Fitch, J., Hopkins, D., Lilly, L., Faeth, R., Falsken, E., and Zdeblick, M., "A Thermopneumatically Actuated Microvalve for Liquid Expansion and Proportional Control," *Solid State Sensors and Actuators*, Vol. 2, Inst. of Electrical and Electronics Engineers, Piscataway, NJ, June 1997, pp. 825–828.

[9] Ketsdever, A., Wadsworth, D., and Muntz, E. P., "Predicted Performance and Systems Analysis of the Free Molecule Micro-Resistojet," *Micropropulsion for Small Spacecraft*, edited by M. Micci and A. Ketsdever, AIAA Progress in Astronautics and Aeronautics, Vol. 187, AIAA, Reston, VA, 2000, pp. 167–183.

[10] Barter, N. J. (ed.), *TRW Space Data*, 5th ed., TRW Space and Electronics Group, Redondo Beach, CA, 1999.

[11] Bauer, H. F., "Fluid Oscillations in the Containers of a Space Vehicle and Their Influence Upon Stability," NASA TR-R-187, Feb. 1964.

[12] O'Brien, W. J., "Capillary Penetration of Liquids Between Dissimilar Solids," Ph.D. Dissertation, Univ. of Michigan, Ann Arbor, MI, Univ. Microfilm No. 6715666, 1967.

[13] Lide, D. R. (ed.), *Handbook of Chemistry and Physics*, 78th ed., CRC Press, Boca Raton, FL, 1997, pp. 6–3.

[14] Jamison, A., Ketsdever, A., and Muntz, E. P., "Gas Dynamic Calibration of a Nano-Newton Thrust Stand," *Review of Scientific Instruments*, Vol. 73, No. 10, 2002, pp. 3629–3637. doi:10.1063/1.1505096

[15] Selden, N., and Ketsdever, A., "Comparison of Force Balance Calibration Techniques for the Nano-Newton Range," *Review of Scientific Instruments*, Vol. 74, No. 12, 2003, pp. 5249–5254. doi:10.1063/1.1623628

[16] Ketsdever, A., "Facility Effects on Performance Measurements of Micropropulsion Systems that Utilize Gas Expansion," *Journal of Propulsion and Power*, Vol. 18, No. 4, 2002, pp. 797–804.

[17] Bird, G. A., *Molecular Gas Dynamics and the Direct Simulation of Gas Flows*, Oxford Univ. Press, Oxford, 1994.

D. Spencer
Associate Editor